

CaS: a key medium for C-O-S-Ca cycles in Earth

Yuegao Liu¹, I-Ming Chou¹, Jiangzhi Chen¹, Nanping Wu¹, Shenghua Mei^{1*} & Liping Wang^{2*}

Oldhamite (CaS) is a rare mineral, which is only observed naturally in enstatite meteorites. No occurrence of CaS has been documented from other groups of meteorites and terrestrial samples¹. However, in experiments at 1.5 GPa/1510 K and 0.5 GPa/1320 K, when the $\lg f_{O_2}$ is lower than -10.57 (FMQ-0.52), CaS was produced in this study by a two-melt mechanism involving the reaction between molten pyrrhotite-pentlandite-bearing orthopyroxenite and molten CaCO_3 . CaS can be easily oxidized to form CaSO_4 or hydrolyzed to produce calcium hydroxide, which may explain why it has never been found in geological samples from Earth. We speculate that part of the anhydrite and gypsum in black smokers along mid-ocean ridges are related to the oxidation or hydrolysis of CaS in the underlying mantle. CaS can be produced when the Siberian mantle plume intruded into the lithosphere.

Enstatite meteorites (EMs), which are the most reduced, undifferentiated extraterrestrial materials and are the only rock type in which oldhamite (CaS) occurs, likely experienced an oxygen fugacity well below IW-2.7 (IW = iron-wüstite redox

¹CAS Key Laboratory for Experimental Study under Deep-sea Extreme Conditions, Institute of Deep-sea Science and Engineering, Chinese Academy of Sciences, Sanya 572000, Hainan, P.R. China.

²Academy for Advanced Interdisciplinary Studies, Southern University of Science and Technology, Shenzhen 518055, Guangdong, P.R. China.

*To whom correspondence should be addressed. E-mail: mei@idsse.ac.cn; wanglp3@sustech.edu.cn.

buffer, in $\lg f_{\text{O}_2}$)². The oxygen-poor signature of EMs suggests that they formed near the center of the solar nebula, i.e., within the orbit of Mercury³. It is widely accepted that CaS formed in a reduced environment. For example, CaS could be a major component of Mercury's surface⁴. However, the formation process of CaS in EMs remains under dispute. There are currently two main views regarding this issue.

Some researchers hold the view that CaS is a product of condensation of the nebula gas. Laboratory smoke experiments demonstrate that pure CaS and a solid solution of CaS and CaO [Ca(S,O)] condense from vapor phase calcium, sulfur, and oxygen with the O/S atomic ratio of <2 and between 2 and 10, respectively⁵. This evidence directly supports a nebular gas origin. Furthermore, according to first-principles calculations, at equilibrium oldhamite is more easily enriched in light Ca isotopes than the other solid minerals; in contrast, condensed Ca-bearing minerals from nebular gas are enriched in heavy Ca isotopes relative to the residual gaseous Ca⁶. Natural oldhamites in EM are isotopically heavier than coexisting silicate materials, indicating that EM oldhamites should have been formed during the condensation of solar nebular gas. However, sulfur isotope data do not support the nebula gas origin. The correlation between $\Delta^{33}\text{S}$ and $\Delta^{36}\text{S}$ of some EMs does not follow the trends of photochemistry in the solar nebula with $\Delta^{36}\text{S} = -2.98\Delta^{33}\text{S}$ ⁷ and of cosmic-ray spallation during presolar nebula with $\Delta^{36}\text{S} = 8\Delta^{33}\text{S}$ ⁸.

Some scholars argue that the oldhamite in EMs is of igneous origin⁹. Textural evidence includes apparent primary igneous grain boundaries between oldhamite and forsterite and the presence of round, droplet-like Mn-Fe-Mg-Cr-Na sulfide inclusions

within oldhamite, which appear to represent an immiscible sulfide liquid⁹. However, the most representative rare earth elements (REE) pattern of oldhamite in EMs is characterized by slight to large positive Eu and Yb anomalies and enrichment in light REEs relative to heavy REEs¹⁰. Nevertheless, experimental petrology studies have shown that¹¹ the Ca-rich sulfide liquid is enriched in the heavy REEs at 1523 K and oxygen fugacity of $\lg f_{\text{O}_2} = -17$. The REE fractionation between the Ca-rich sulfide liquid and the silicate liquid (D value) is extreme, with $D(\text{Lu}) = 60 * D(\text{La})$ at 1473 K¹¹. This finding is at odds with an igneous origin.

In current study, after reaction between pyrrhotite-pentlandite-bearing orthopyroxenite (PPO) and CaCO_3 in a graphite-lined $\text{Au}_{75}\text{Pd}_{25}$ capsule (Fig. 1a) in two experiments conducted at 1.5 GPa/1510 K and 0.5 GPa/1320 K, oldhamites were observed at the central reaction zone in recovered samples (Figs. 1b, 1c, and S3). That is, oldhamite appears to have formed during interaction of carbonate melt and sulfide-bearing silicate melt at suitable $P\text{-}T\text{-}f_{\text{O}_2}$ conditions. Here, we name this formation process the two-melt mechanism. In the absence of calcium carbonate, the magmas produced by the partial melting of orthopyroxenite under two $P\text{-}T$ conditions are similar in composition, and both are high-magnesium basaltic magmas ($\text{SiO}_2 = 54.5\text{--}54.9$ wt.%, $\text{MgO} = 9.54\text{--}10.19$ wt.%; [Methods section and Supplementary Table 3](#)). Basaltic melts are common at mid-ocean ridges and large igneous provinces. Oxygen fugacity in graphite-lined noble metal capsule is about $\text{FMQ} - 2.2$ ¹² ($\text{FMQ} =$ fayalite-magnetite-quartz redox buffer). These $P\text{-}T\text{-}f_{\text{O}_2}$ experimental conditions for CaS formation are considered to be easily achieved inside the Earth; the two-melt

mechanism can occur during carbonate melt metasomatism in the mantle and the intrusion of mantle-derived magma into the lithosphere. The outward ring structure in the order of $\text{Ca}(\text{OH})_2$, CaS , and pentlandite were found in meteorites¹³. Thus, these researchers propose that CaCO_3 thermally decomposed into CaO , which reacted with the sulfur ion to form CaS ¹³. In this study, some sulfides occurred around CaS , and bubbles are always present close to CaS (Fig. 1b and Fig. S3). Therefore, the most probable route for the CaS formation is: CaCO_3 (melt) = CaO (melt) + CO_2 (gas), CaO (melt) + FeS (melt) = CaS (solid) + FeO (melt).

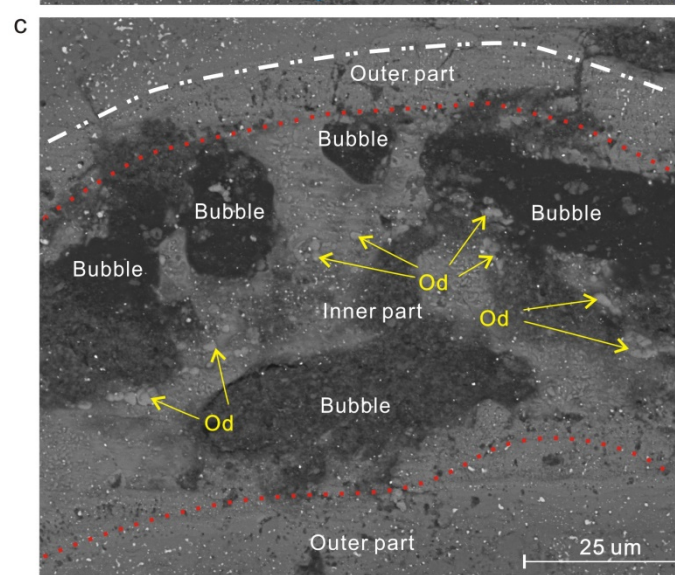
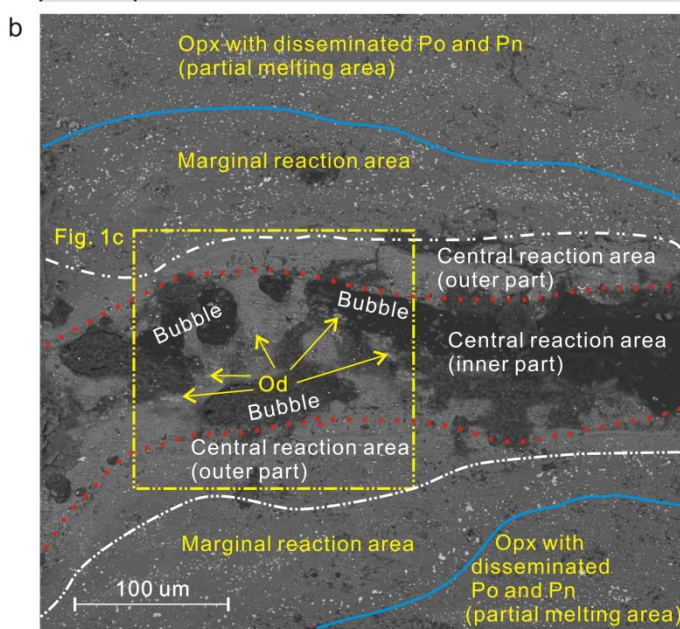
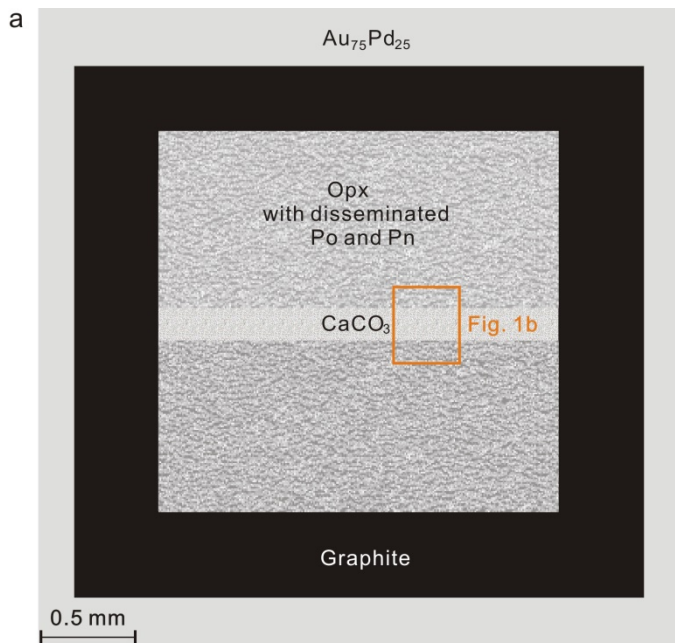
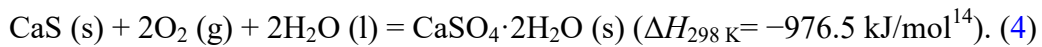
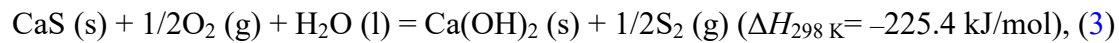
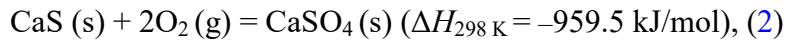
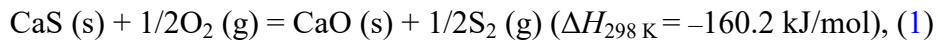


Figure 1. State and location of CaS generated by the two-melt mechanism.

a. Reaction chamber for the contamination experiments between the Po-Pn-bearing orthopyroxenite and CaCO_3 ; **b.** General view of scanning electron microscope image after contamination experiment No. C1 at 0.5 GPa and 1320 K; average composition of Cpx, Opx, and melts at different reaction zone are listed in [Supplementary Table 5](#).

c. Drop-shaped CaS in the inner part of the central reaction zone and disseminated Fe-Ni sulfide (bright white). Opx = orthopyroxenite, Po = pyrrhotite, Pn = pentlandite, and Od = oldhamite.

To date, no occurrence of CaS in natural terrestrial samples has been reported, probably due to the following reactions occurred:



That is, CaS can be easily oxidized to form calcium sulfate. Moreover, in the presence of H_2O , CaS can be hydrolyzed to form calcium hydroxide. Thus, whether the CaS generated by magmatism inside a planet can be preserved on the surface of the planet is related to at least three factors (1) oxygen fugacity of the magma; (2) oxygen content in the atmosphere; (3) H_2O content on the planet surface.

Oxygen fugacity at the oldhamite–anhydrite equilibrium (Eq. 2, named [OA buffer](#)) and the oldhamite–lime equilibrium (Eq. 1, named [OL buffer](#)) can be

determined by Eqs. 5 and 6, respectively (Method section):

$$\lg f_{\text{O}_2} = 2.19144 + 1.09305 \times 10^{-4} T - 25137/T - 1551.42/T^2 + 1.5305 \times 10^7/T^3 + 0.04777P/T + 2.78381\lg T, \quad (5)$$

$$\lg f_{\text{O}_2} = -21.1162 + 3.65342 \times 10^7/T^3 - 6205.07/T^2 + (-16237.94 - 0.11450P)/T + 0.43722 \times 10^{-3}T + 11.13544\lg T + \lg f_{\text{S}_2}, \quad (6)$$

where P is pressure in bar, and T is temperature in K.

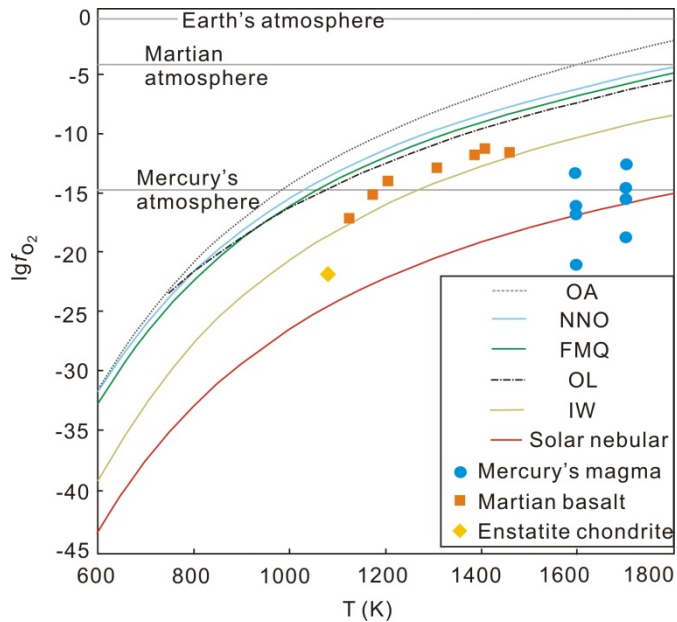


Figure 2. Representative oxygen fugacity buffer vs. temperature curves typically used in geochemistry, including IW ($\text{Fe} + \frac{1}{2}\text{O}_2 = \text{FeO}$), FMQ ($3\text{Fe}_2\text{SiO}_4 + \text{O}_2 = 2\text{Fe}_3\text{O}_4 + 3\text{SiO}_2$), and NNO ($\text{Ni} + \frac{1}{2}\text{O}_2 = \text{NiO}$), are shown together with OL ($\text{CaS (s)} + \frac{1}{2}\text{O}_2 (\text{g}) = \text{CaSO}_4 (\text{s})$) at 0.5 GPa total pressure. References: NNO is from O'Neill (1987a)¹⁵, and FMQ and IW are from O'Neill (1987b)¹⁶; $\lg f_{\text{S}_2}$ value of -12 (mean sulfur fugacity of black smoker¹⁷) was used during the OL calculation. $\lg f_{\text{O}_2}$ of solar nebula is calculated by the equation

$\lg f_{\text{O}_2} = -0.85 - 25,664/T$, where T is in K¹⁸. The $\lg f_{\text{O}_2}$ values of enstatite chondrite, Martian basalt, and the silicate melts on the Mercury's surface are from Brett and Sato (1984)², Herd et al. (2002)¹⁹, and Zolotov et al. (2013)²⁰, respectively.

CaS is stable when $\lg f_{\text{O}_2}$ is below OL buffer but cannot exist when $\lg f_{\text{O}_2}$ is above OA buffer. At 0.5 GPa and 1320 K, OA = FMQ + 2.21 ($\lg f_{\text{O}_2} = -7.83$) and OL = FMQ - 0.52 ($\lg f_{\text{O}_2} = -10.57$) (Fig. 2). The $\lg f_{\text{O}_2}$ value of Mercury's surface magma ranges from IW-2.93 to IW-10.5 ($\lg f_{\text{O}_2} = -13.2$ to -21.7) at 1600–1700 K (Fig. 2), and the $\lg f_{\text{O}_2}$ value of Mercury's atmosphere is -14.7. These values are much lower than the OL buffer (Fig. 2), and no H₂O has been found in the atmosphere and on the surface of Mercury, which probably are the reasons why CaS could be preserved on Mercury. Although $\lg f_{\text{O}_2}$ of Martian magma is significantly lower than OL, due to the existence of H₂O on Mars and high $\lg f_{\text{O}_2}$ value (-4.32) of the Martian atmosphere (Fig. 2), which is significantly higher than OA below 1500 K, no CaS but some sulfate has been found on Mars. The average $\lg f_{\text{O}_2}$ values for arc basalts, ocean island magma, and most basalt related to mantle plume on Earth are FMQ + 0.96, FMQ + 0.82, and FMQ + 0.1, respectively²¹, which are higher than OL. Moreover, the $\lg f_{\text{O}_2}$ value of -0.67 of Earth's atmosphere is much higher than OA (Fig. 2), and H₂O widely exist in Earth's crust. The above environments are not conducive to the preservation of CaS in terrestrial samples. However, we believe that CaS can exist in the interior of the Earth and transiently in certain Earth surface environments.

The possible existence of CaS in mantle inclusions

Native Fe, native Ni, and numerous anhydrite inclusions were identified in diamonds from the Juina area, Brazil²². Anhydrite has also been reported as inclusions in kyanite from crustal-type eclogites from the Dabie-Sulu ultra-high pressure metamorphic belt, where diamond has been discovered^{23,24}. When oxygen fugacity is lower than FMQ-1, there is almost no S⁶⁺ in the melt²⁵. The upper limit of the oxygen fugacity for diamond formation in the mantle is FMQ-1.5²⁶. Thus, it is nearly impossible that sulfate exists during the diamond formation process. A reasonable explanation is that the primary inclusion component was CaS, which could have reacted with O₂ to form anhydrite during the ascending and exhumation of the host rocks.

The possible transient presence of CaS in the Siberian large igneous province

The Siberian large igneous province (SLIP) at the Permian-Triassic boundary (PTB) is dominated by low magnesium (MgO < 7 wt. %) tholeiitic basalts and contains minor olivine basalts and picrites²⁷. This composition is roughly similar to the composition of the initial melt formed by the partial melting of orthopyroxenite in this research ([Supplementary Table 3](#)). The average lgfo₂ of magma erupting at and around the mantle plumes of Hawaii, Erebus, Iceland, and the Canary Islands is FMQ + 0.1²¹. However, the Siberian mantle plume is characterized by much lower oxygen fugacity. The average oxygen fugacity of primary melts of Gudchikhinsky Formation on the surface in the SLIP is FMQ-1.5²⁷. Abundant coal- and petroleum-bearing carbonates occur in or around the SLIP. Carbon contamination is widespread in SLIP²⁸, reducing the oxygen fugacity of magma so much that even native Fe appears²⁹, which only

occurs if the oxygen fugacity is less than FMQ-4.5 (Fig. 2). However, magmatic anhydrites have been found in some intrusions in the SLIP despite prevailing reducing environment³⁰. Thus, it is conceivable that the CaS formation via the two-melt mechanism occurred during the intrusion of mantle plume in the SLIP.

Moreover, large quantities of anhydrite and gypsum layers and anhydrite-containing rocks exist in or around the SLIP with the visible thickness of some anhydrite layers reaching 25 m on surface³¹. Most scholars hold the view that anhydrite contamination promoted the formation of the world's largest magmatic Cu-Ni deposit^{28,32}. When CaSO₄ encounters such a reducing magma with $\lg f_{\text{O}_2}$ value from FMQ-1.5 to FMQ-4.5, hexavalent S can no longer exist. In the modern industry, CaS is produced by the reaction of C and CaSO₄ ($\text{CaSO}_4 + 2\text{C} = \text{CaS} + 2\text{CO}_2$) in the temperature range of 1023–1353 K³³. Under the condition that CO, N₂, and CO₂ are mixed as reducing agents, through the reaction $\text{CaSO}_4 + 4\text{CO} = \text{CaS} + 4\text{CO}_2$ at 923 K, the generation efficiency of CaS is 95%³⁴. These two reactions likely proceeded during the interaction between the carbon-contaminated Siberian magma and the surrounding anhydrite rocks. When the lava cooled, CaS can be easily oxidized to form CaSO₄. In this process, one CO₂ molecule is produced with one or one half O₂ molecule removed from the atmosphere. The transient presence of CaS may have played a role in raising CO₂ content and lowering O₂ content in the atmosphere at PTB.

The link between CaS and anhydrite in black smokers

In the mantle below a mid-ocean ridge, at a depth of about 160–170 km, diamond would transform to graphite if the oxygen fugacity is above FMQ–2^{35,36} (Fig. 3). Redox melting [C (graphite) + 2Fe₂O₃ (melt) + O²⁻ (melt) = 4FeO + CO₃²⁻ (both in the melt)]³⁷ occurs mainly at a depth of 120–150 km³⁶. The carbonate melt produced by redox melting will ascend as a flux into the overlying mantle and react with mantle silicates to stabilize a carbonated silicate melt³⁸ (Fig. 3). At a depth of about 60 km, the carbonate melt evolves towards a silicate melt composition³⁶. The mid-ocean ridge basalt (MORB), at the top location of the silicate melt, is characterized by a redox state of FMQ–0.41³⁹ (Fig. 3). Within the mantle bounded by the diamond-to-graphite interface and location of MORB, CaS is stable (i.e., below OL), and carbonate and basaltic melts are common. Thus, it is reasonable to speculate that the formation of CaS is possible (Fig. 3). Large amounts of anhydrite and gypsum exist in black smokers along mid-ocean ridges (BSMOR)⁴⁰ (Fig. 3), which is considered to be derived from seawater as the δ³⁴S_{V-CDT} values of these sulfates are nearly the same to that of modern seawater⁴¹. The δ³⁴S_{V-CDT} of modern seawater sulfate is 21.24‰⁴². However, the δ³⁴S_{V-CDT} value of anhydrite gradually decreases from the seawater's 20 ± 1‰ to 3.4‰, while ⁸⁷Sr/⁸⁶Sr value of anhydrite decrease downward from the seawater value of 0.7088 to a MORB value of 0.7029 in a 1.8 km deep drillhole for the ocean-ridge black smoker systems^{43,44}. The S and Sr sources from the MORB beneath the black smoker are attributed to anhydrite. The δ³⁴S_{V-CDT} value of 3.4‰ is much lower than that of modern seawater, which is considered to result from the

oxidation of low- $\delta^{34}\text{S}$ sulfide to sulfate during the fluid extractions in the basalt basement⁴⁵. CaS is easily oxidized or hydrolyzed, due to the large negative $\Delta H_{298\text{K}}$ for the reactions 2, 4, and 5. As CaS can exist in the mantle region beneath a mid-ocean ridge, it may serve as a source for anhydrite and gypsum in BSMOR (Fig. 3).

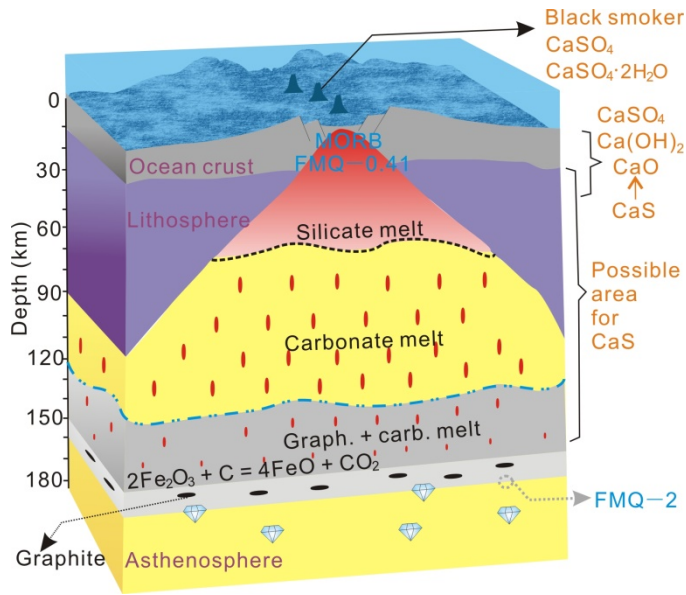


Figure 3. Possible area for the existence and evolution of CaS beneath a mid-ocean ridge. At a depth of 160–170 km, the transformation from diamond to graphite occurs if the oxygen fugacity is above FMQ-2³⁶. At a depth of $150 \pm 50 \text{ km}$ ³⁶, ‘redox melting’ [$\text{C} (\text{graphite}) + 2\text{Fe}_2\text{O}_3 (\text{melt}) + \text{O}^{2-} (\text{melt}) = 4\text{FeO} + \text{CO}_3^{2-}$ (both in the melt)]³⁷ takes place over a depth interval of 30 km, over which 30 ppm of carbon in the mantle source is oxidized³⁶. The ascending carbonate melt acts as a flux to the overlying mantle and reacts with the mantle silicates to stabilize a carbonated silicate melt³⁸. At a depth of 60 km, the carbonate melt evolves toward a silicate melt composition³⁶.

1 Defouilloy, C., Cartigny, P., Assayag, N., Moynier, F. & Barrat, J. A. High-precision sulfur
isotope composition of enstatite meteorites and implications of the formation and evolution of
their parent bodies. *Geochimica et Cosmochimica Acta* **172**, 393–409 (2016).

2 Brett, R. & Sato, M. Intrinsic oxygen fugacity measurements on seven chondrites, a pallasite,
and a tektite and the redox state of meteorite parent bodies. *Geochimica et Cosmochimica
Acta* **48**, 111–120 (1984).

3 Kallenbach, R. *et al.* in *Solar System History from Isotopic Signatures of Volatile Elements*.
(eds R Kallenbach *et al.*) 413–422 (Springer Science & Business Media).

4 Bennett, C. J. *et al.* Investigating potential sources of Mercury's exospheric Calcium:
Photon-stimulated desorption of Calcium Sulfide. *Journal of Geophysical Research: Planets*
121, 137–146 (2016).

5 Yokoyama, K., Kimura, Y. & Kaito, C. Experiments on condensation of calcium sulfide grains
to demarcate environments for the formation of enstatite chondrites. *ACS Earth and Space
Chemistry* **1**, 601–607 (2017).

6 Huang, F., Zhou, C., Wang, W., Kang, J. & Wu, Z. First-principles calculations of equilibrium
Ca isotope fractionation: Implications for oldhamite formation and evolution of lunar magma
ocean. *Earth and Planetary Science Letters* **510**, 153–160 (2019).

7 Chakraborty, S., Jackson, T. L., Ahmed, M. & Thiemens, M. H. Sulfur isotopic fractionation
in vacuum UV photodissociation of hydrogen sulfide and its potential relevance to meteorite
analysis. *Proceedings of the National Academy of Sciences* **110**, 17650–17655 (2013).

8 Farquhar, J., Jackson, T. L. & Thiemens, M. H. A ^{33}S enrichment in ureilite meteorites:
evidence for a nebular sulfur component. *Geochimica et Cosmochimica Acta* **64**, 1819–1825
(2000).

9 Wheelock, M. M., Keil, K., Floss, C., Taylor, G. & Crozaz, G. REE geochemistry of
oldhamite-dominated clasts from the Norton County aubrite: Igneous origin of oldhamite.
Geochimica et Cosmochimica Acta **58**, 449–458 (1994).

10 Gannoun, A., Boyet, M., El Goresy, A. & Devouard, B. REE and actinide microdistribution in
Sahara 97072 and ALHA77295 EH3 chondrites: A combined cosmochemical and petrologic
investigation. *Geochimica et Cosmochimica Acta* **75**, 3269–3289 (2011).

11 Jones, J. & Boynton, W. Experimental geochemistry in very reducing systems: Extreme REE
fractionation by immiscible sulfide liquids. in *Lunar and planetary science conference*.
353–354.

12 Médard, E., Mccammon, C. A., Barr, J. A. & Grove, T. L. Oxygen fugacity, temperature
reproducibility, and H_2O contents of nominally anhydrous piston-cylinder experiments using
graphite capsules. *American Mineralogist* **93**, 1838–1844 (2008).

13 Haberle, C. W. & Garvie, L. A. Extraterrestrial formation of oldhamite and portlandite through
thermal metamorphism of calcite in the Sutter's Mill carbonaceous chondrite. *American
Mineralogist* **102**, 2415–2421 (2017).

14 Robie, R. A. & Hemingway, B. S. *Thermodynamic properties of minerals and related
substances at 298.15 K and 1 bar (10^5 Pascals) pressure and at higher temperatures*. U.S.
Geological Survey Bulletin edn, 461 (US Government Printing Office, 1995).

15 O'Neill, H. S. Free energies of formation of NiO , CoO , Ni_2SiO_4 , and Co_2SiO_4 . *American
Mineralogist* **72**, 280–291 (1987).

16 O'Neill, H. S. Quartz-fayalite-iron and quartz-fayalite-magnetite equilibria and the free energy

of formation of fayalite (Fe_2SiO_4) and magnetite (Fe_3O_4). *American Mineralogist* **72**, 67–75 (1987).

17 Keith, M. *et al.* Effects of temperature, sulfur, and oxygen fugacity on the composition of sphalerite from submarine hydrothermal vents. *Geology* **42**, 699–702 (2014).

18 Krot, A. N., Fegley Jr, B., Lodders, K. & Palme, H. Meteoritical and astrophysical constraints on the oxidation state of the solar nebula. *Protostars and planets IV* **1019** (2000).

19 Herd, C. D., Borg, L. E., Jones, J. H. & Papike, J. J. Oxygen fugacity and geochemical variations in the Martian basalts: Implications for Martian basalt petrogenesis and the oxidation state of the upper mantle of Mars. *Geochimica et Cosmochimica Acta* **66**, 2025–2036 (2002).

20 Zolotov, M. Y. *et al.* The redox state, FeO content, and origin of sulfur-rich magmas on Mercury. *Journal of Geophysical Research: Planets* **118**, 138–146 (2013).

21 Cottrell, E. *et al.* Oxygen fugacity across tectonic settings. *Magma Redox Geochemistry*, 33–61 (2021).

22 Wirth, R., Kaminsky, F., Matsyuk, S. & Schreiber, A. Unusual micro-and nano-inclusions in diamonds from the Juina Area, Brazil. *Earth and Planetary Science Letters* **286**, 292–303 (2009).

23 Hwang, S. L. *et al.* Crust-derived potassic fluid in metamorphic microdiamond. *Earth and Planetary Science Letters* **231**, 295–306 (2005).

24 Zhang, Z. M. *et al.* Fluids in deeply subducted continental crust: petrology, mineral chemistry and fluid inclusion of UHP metamorphic veins from the Sulu orogen, eastern China. *Geochimica et Cosmochimica Acta* **72**, 3200–3228 (2008).

25 Jugo, P. J., Luth, R. W. & Richards, J. P. Experimental data on the speciation of sulfur as a function of oxygen fugacity in basaltic melts. *Geochimica et Cosmochimica Acta* **69**, 497–503 (2005).

26 Stagno, V., Frost, D., McCammon, C., Mohseni, H. & Fei, Y. The oxygen fugacity at which graphite or diamond forms from carbonate-bearing melts in eclogitic rocks. *Contributions to Mineralogy and Petrology* **169**, 16 (2015).

27 Sobolev, A. V., Krivolutskaya, N. A. & Kuzmin, D. Petrology of the parental melts and mantle sources of Siberian trap magmatism. *Petrology* **17**, 253–286 (2009).

28 Lacono-Marziano, G., Ferraina, C., Gaillard, F., Carlo, I. D. & Arndt, N. T. Assimilation of sulfate and carbonaceous rocks: experimental study, thermodynamic modeling and application to the Noril'sk-Talnakh region (Russia). *Ore Geology Reviews* **90**, 399–413 (2017).

29 Ryabov, V. & Lapkovsky, A. Native iron (–platinum) ores from the Siberian Platform trap intrusions. *Australian Journal of Earth Sciences* **57**, 707–736 (2010).

30 Li, C., Ripley, E. M., Naldrett, A. J., Schmitt, A. K. & Moore, C. H. Magmatic anhydrite-sulfide assemblages in the plumbing system of the Siberian Traps. *Geology* **37**, 259–262 (2009).

31 Ryabov, V., Shevko, A. Y. & Gora, M. *Trap magmatism and ore formation in the Siberian Noril'sk region*. Vol. 2 (Springer, 2014).

32 Sobolev, S. V. *et al.* Linking mantle plumes, large igneous provinces and environmental catastrophes. *Nature* **477**, 312–316 (2011).

33 Van der Merwe, E., Strydom, C. & Potgieter, J. Thermogravimetric analysis of the reaction between carbon and $\text{CaSO}_4 \cdot 2\text{H}_2\text{O}$, gypsum and phosphogypsum in an inert atmosphere.

34 *Thermochim. Acta* **340**, 431–437 (1999).

35 Li, H. & Zhuang, Y. Catalytic reduction of calcium sulfate to calcium sulfide by carbon monoxide. *Industrial & Engineering Chemistry Research* **38**, 3333–3337 (1999).

36 Stagno, V. & Frost, D. J. Carbon speciation in the asthenosphere: Experimental measurements of the redox conditions at which carbonate-bearing melts coexist with graphite or diamond in peridotite assemblages. *Earth and Planetary Science Letters* **300**, 72–84 (2010).

37 Stagno, V., Ojwang, D. O., McCammon, C. A. & Frost, D. J. The oxidation state of the mantle and the extraction of carbon from Earth's interior. *Nature* **493**, 84–88 (2013).

38 Kadik, A. Evolution of Earth's redox state during upwelling of carbon-bearing mantle. *Physics of the Earth and Planetary Interiors* **100**, 157–166 (1997).

39 Dasgupta, R. & Hirschmann, M. M. The deep carbon cycle and melting in Earth's interior. *Earth and Planetary Science Letters* **298**, 1–13 (2010).

40 Bézos, A. & Humler, E. The $\text{Fe}^{3+}/\Sigma\text{Fe}$ ratios of MORB glasses and their implications for mantle melting. *Geochimica et Cosmochimica Acta* **69**, 711–725 (2005).

41 Humphris, S. E. *et al.* The internal structure of an active sea-floor massive sulphide deposit. *Nature* **377**, 713–716 (1995).

42 Styrt, M. *et al.* The mineralogy and the isotopic composition of sulfur in hydrothermal sulfide/sulfate deposits on the East Pacific Rise, 21 °N latitude. *Earth and Planetary Science Letters* **53**, 382–390 (1981).

43 Tostevin, R. *et al.* Multiple sulfur isotope constraints on the modern sulfur cycle. *Earth & Planetary Science Letters* **396**, 14–21 (2014).

44 Teagle, D. A., Alt, J. C. & Halliday, A. N. Tracing the chemical evolution of fluids during hydrothermal recharge: Constraints from anhydrite recovered in ODP Hole 504B. *Earth and Planetary Science Letters* **155**, 167–182 (1998).

45 Teagle, D. A., Bickle, M. J. & Alt, J. C. Recharge flux to ocean-ridge black smoker systems: a geochemical estimate from ODP Hole 504B. *Earth and Planetary Science Letters* **210**, 81–89 (2003).

46 Alt, J. C., Zuleger, E. & Erzinger, J. Mineralogy and stable isotopic compositions of the hydrothermally altered lower sheeted dike complex, Hole 504B, Leg 140. in *Proceedings of the Ocean Drilling Program, Scientific Results* **137**, 155–166 (1995).